Z. Kristallogr. 219 (2004) 278–294

Structural variation and crystal chemistry of $LiMe^{3+}Si_2O_6$ clinopyroxenes Me^{3+} = Al, Ga, Cr, V, Fe, Sc and In

Günther J. Redhammer* and Georg Roth

Institute of Crystallography, Rheinisch-Westfälische Technische Hochschule (RWTH) Aachen, Jägerstraße 17/19, D-52056 Aachen, Germany

Received February 17, 2003; accepted February 11, 2004

Li–clinopyroxenes / Crystal chemistry / Single crystal structure analysis / X-ray diffraction

Abstract. A total of 32 synthetic end-member and solid-solution compounds of the $LiM^{3+}Si_2O_6$ (Li = M2 site, M^{3+} = M1 site = Al, Ga, V, Fe, Sc and In) clinopyroxene series have been investigated by single-crystal X-ray diffraction. Except $LiCrSi_2O_6$, all compounds show *C2/c* symmetry at 295 K. $LiCrSi_2O_6$ has space group $P2_1/c$ but transforms to the high temperature *C2/c* structure at 335 K. The variations of structural parameters in the $LiMe^{3+}Si_2O_6$ clinopyroxenes are dominated by the Me^{3+} site. The average M1–O bond length is linearly correlated with the ionic radius of the M1 cation. Octahedra reflect the increasing size of the M1 cations by steadily increasing bond and edge lengths, the variations however are not uniform. With increasing size of the M1 cation, octahedra deviate from ideal octahedral geometry. Octahedral edges, shared with other structural units, are distinctly hampered in expansion with increasing size of the M1 cation. The increasing size of the M1 octahedral chain is compensated by changing the kinking of the tetrahedral chain and by alterations of bond and edge lengths as well as the bond angles within the tetrahedron. Three different mechanisms of adapting of the structural building units with increasing M^{3+} cationic radius can be identified: (i) expansion of the tetrahedral chain by stretching (ii) transition form "O" to "S" chain conformation after full expansion and (iii) finally a limit of expansion in *a* direction. We stress that cations larger than In^{3+} cannot be substituted at the M1 site because of too large geometrical differences between octahedral and tetrahedral chains.

Introduction

The structure of the clinopyroxenes is very flexible and accepts a variety of cations, particularly on the octahedral M1 site. Hence, this mineral group appears to be well suited for a systematic study of structural changes over a wide range of compositions, most of which do not occur as minerals. For the Lithium-pyroxenes $LiM^{3+}Si_2O_6$ with Li = M2 site and M^{3+} = M1 site, only spodumene α-$LiAlSi_2O_6$ is found in nature, however, synthetic compounds with M^{3+} = Ga, Cr, Fe, V, Sc and In are known to exist.

Ito and Frondel (1968) were the first to synthesise the Sc^{3+} analog of spodumene, while the Li-pyroxenes with M^{3+} = V, Cr, and Fe first were described by Brown (1971) who used dry synthesis experiments near 1000 °C. Later Drysdale (1975) reported the hydrothermal synthesis of compounds with M^{3+} = Fe, Cr, V, Sc and In. Behruzi, Banerjea-Appel, Hahn and Scherberich (1984a) synthesised single crystals of $LiFeSi_2O_6$ and $LiCrSi_2O_6$ by using a high-temperature flux growth technique. A similar method was used by Grotepaß, Behruzi and Hahn (1983) to grow $LiScSi_2O_6$ and $LiInSi_2O_6$ single crystals. Very recently Redhammer, Roth, Paulus, André, Lottermoser, Amthauer, Treutmann, Koppelhuber-Bitschnau (2001) produced single crystals of $LiFeSi_2O_6$ by high-temperature/high-pressure synthesis at 1573 K and 2.5 GPa.

Lithium-pyroxenes are chain silicates and have monoclinic symmetry (freqeuntly *C2/c*) at room temperature. The structure consists of alternating chains of SiO_4 tetrahedra and ribbons of edge-sharing M1–O-octrahedra (containing the M^{3+} cation) linked via common edges to irregular M2-polyhedra with six-fold oxygen-coordination (containing the Li^+ cation). The chains and ribbons are running along the crystallographic *c*-axis. Figure 1 shows a representation of the crystal structure of $LiCrSi_2O_6$ as an example.

The structures of $LiAlSi_2O_6$ and $LiFeSi_2O_6$ were first investigated by Clark, Appleman and Papike (1969). Hawthorne and Grundy (1977) determined the structure of $LiScSi_2O_6$, and Behruzi, Hahn, Prewitt and Baldwin (1984b) found that $LiCrSi_2O_6$ crystallises in space group $P2_1/c$ at room temperature. Grotepaß et al. (1983) determined the crystal structure of $LiInSi_2O_6$. However, structural information given by Behruzi et al. (1984b) and Grotepaß et al. (1983) is very limited (e.g. no fractional atomic coordinates, bond lengths and angles). $LiGaSi_2O_6$ and $LiVSi_2O_6$ have been investigated by single-crystal methods by Sato, Osawa and Ohasi (1994) and by Satto, Millet and Galy (1997) respectively. Very recently Ohashi (2003) presented structural details on a large number of alkali-clinopyroxenes including the solid solution series

* Correspondence author (e-mail: guenther.redhammer@aon.at)

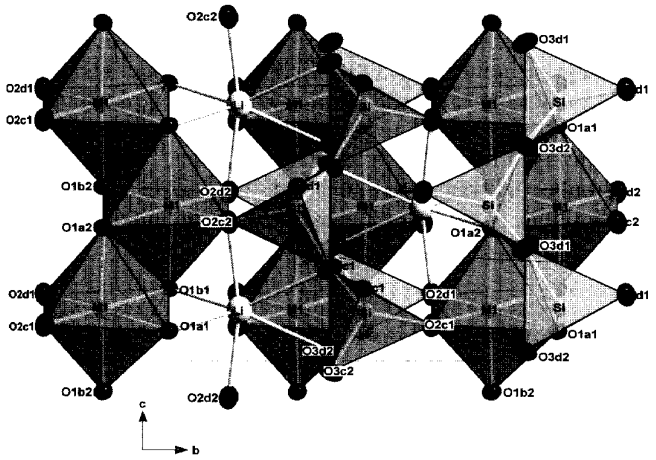

Fig. 1. Structure of $LiCrSi_2O_6$, viewed approximately along the *a*-axis. The labelling of atoms is chosen according Burnham, Clark, Papike and Prewitt (1967)

Li(Al, Ga)Si_2O_6 and Kopnin, Sato and Takayama-Muromachi (2003) gave first structural details on the compound $LiTiSi_2O_6$.

Besides all the published work, there is no detailed crystal chemical consideration of the complete Li-pyroxene series up to now. Thus in the present study, we have synthesised a series of end-member compositions $LiM^{3+}Si_2O_6$ with Me^{3+} = Al, Ga, Cr, Fe, V, Sc, and In as well as compounds on the $Li(Fe_{1-x}Sc_x)Si_2O_6$ and $Li(Sc_{1-x}In_x)Si_2O_6$ solid solution series and subsequently investigated these samples by single-crystal X-ray diffraction in order to (i) refine the structures of $LiCrSi_2O_6$ and $LiInSi_2O_6$ and (ii) to give a improved and refined crystal chemical description of $LiMe^{3+}Si_2O_6$ clinopyroxenes, not available so far in the literature. A study of the low temperature (80 K $\leq T \leq$ 296 K) structural properties of the samples investigated here is presented in a companion paper (Redhammer and Roth, 2004).

Sample material and experimental

Single crystals of $LiAlSi_2O_6$, $LiGaSi_2O_6$, $LiFeSi_2O_6$ and $LiScSi_2O_6$ were prepared from mixtures of Li_2CO_3, Al_2O_3, Ga_2O_3, Fe_2O_3 or Sc_2O_3 and SiO_2 in the stoichiometry of the desired composition (Table 1). The finely ground start-

Table 1. Details on single-crystal growth experiments.

Composition	run	*x*	method	*T* (K)	rate	*P* (GPa)	*t* (h)
$LiAlSi_2O_6$	LiAl	–	HP	1573	–	2.5	81
$LiGaSi_2O_6$	LiGa	–	HP	1573	–	2.5	78
$LiVSi_2O_6$	LiV	–	HP	973	–	0.4	237
$LiCrSi_2O_6$	LiCr	–	flux	1373 → 973	6 K/h	0.0001	103
$LiFeSi_2O_6$	LiHP	–	HP	1573	–	3.0	97
$Li(Fe_{1-x}Sc_x)Si_2O_6$ solid solution series:							
	ScFe90	0.10	flux	1373 → 973	6 K/h	0.0001	73
	ScFe75	0.18	flux	1373 → 973	6 K/h	0.0001	73
	ScFe80	0.44	flux	1373 → 973	6 K/h	0.0001	73
	ScFe70	0.26	flux	1373 → 973	6 K/h	0.0001	69
	ScFe50b	0.29	flux	1373 → 973	6 K/h	0.0001	70
	ScFe50	0.43	flux	1373 → 973	6 K/h	0.0001	77
	ScFe40	0.62	flux	1373 → 973	6 K/h	0.0001	70
	ScFe25	0.91	flux	1373 → 973	6 K/h	0.0001	70
	ScFe20	0.94	flux	1373 → 973	6 K/h	0.0001	70
	ScFe10	0.98	flux	1373 → 973	6 K/h	0.0001	72
	LiSc2	1.00	flux	1373 → 973	6 K/h	0.0001	72
	ScPx	1.00	HP	1573	–	2.5	65
$Li(Sc_{1-x}In_x)Si_2O_6$ solid solution series:							
	LiIn10	0.06	flux	1373 → 973	6 K/h	0.0001	70
	LiIn25	0.20	flux	1373 → 973	6 K/h	0.0001	70
	LiIn35	0.26	flux	1373 → 973	6 K/h	0.0001	70
	LiIn50	0.30	flux	1373 → 973	6 K/h	0.0001	70
	LiIn65	0.55	flux	1373 → 973	6 K/h	0.0001	74
	LiIn90	0.82	flux	1373 → 973	6 K/h	0.0001	71
	LiIn100	1.00	flux	1373 → 973	6 K/h	0.0001	70

HP = high-pressure experiments; flux = high temperature solvent growth using Li_2MoO_4 as a solvent (flux to nutrient = 10 : 1);
x = actual composition from refinement of the M1 site;
rate = cooling rate.

ing materials were filled into small platinum tubes, tightly welded and subjected to a temperature of 1573 K and a pressure of 2.5 GPa over a period of 3–4 days in an in-house built Piston-cylinder-apparatus. These experiments lead to a few milligrams of small prismatic single crystals up to 0.07 mm in length for Me^{3+} = Al, Ga, Sc and up to 0.15 mm for $LiFeSi_2O_6$.

Single crystals of $LiCrSi_2O_6$, $LiScSi_2O_6$ (for comparison with the samples grown at high pressure), $LiInSi_2O_6$ and compounds of the $Li(Fe_{1-x}Sc_x)Si_2O_6$ and of the $Li(Sc_{1-x}In_x)Si_2O_6$ solid solution series (Table 1) were prepared from stoichiometric mixtures of $LiCO_3$, Cr_2O_3, Sc_2O_3, In_2O_3 or Fe_2O_3 and SiO_2 in the desired composition by using a high-temperature solution (flux) growth technique. One part by weight of the finely ground starting material was mixed with ten parts by weight of the high-temperature solvent Li_2MoO_4 and filled into an open platinum crucible, which was then closed with a crimped Pt-cover. The mixture was slowly heated to 1373 K, equilibrated at this temperature for 24 hours and subsequently cooled down to 973 K at a rate of 6 K/hour. Li_2MoO_4 can easily be removed from the product by dissolution in boiling water. The resulting products consisted of prismatic to needle-shaped clinopyroxene crystals up to $0.05 \times 0.05 \times 3.5$ mm in size and small amounts of $Li_2Si_2O_5$. Using ^{57}Fe Mössbauer spectroscopy, selected samples were checked for the valence of iron and in all cases Fe^{3+} was found exclusively.

All attempts to substitute cations larger than In^{3+}, e.g. Y^{3+} on the M1 site, both by high-temperature/high-pressure experiments and by flux growth techniques failed. Also, we were not able to obtain single crystals of the $LiAlSi_2O_6$–$LiGaSi_2O_6$ solid solution.

The sample of $LiVSi_2O_6$ was synthesised hydrothermally at 973 K and a pressure of 0.4 GPa from a stoichiometric mixture of Li_2CO_3, V_2O_3 and SiO_2. The sample material together with ≈10 wt% H_2O was filled into an $Ag_{70}Pd_{30}$ tube, tightly welded and placed in a cold-sealed pressure vessel. The redox-conditions of the pressure-vessel (close to the nickel/nickeloxide solid state oxygen buffer) were used to control the oxidation state of V^{3+} during the experiment. The product of the run consisted of aggregates of grass-green needles of $LiVSi_2O_6$, about $0.02 \times 0.02 \times 2.0$ mm in size.

Selected single crystals from the synthesis experiments with a minimum of twinning (less than 5% of the second individual, see below) were used for subsequent structure refinement by X-ray diffraction. Although more than 20 crystals had been tested for each composition, not a single one is absolutely free of polysynthetic twinning. More detailed comments on this twinning are given in Redhammer and Roth (2002). The single-crystal X-ray diffraction data sets were collected on an imaging-plate diffractometer system (Stoe-IPDS, MoK_α radiation, pyrolytic graphite monochromator). The programs X-SHAPE (Stoe & Cie, 1996) and SHELXL (Sheldrick, 1997) were used for empirical absorption correction via reflection intensity equivalents and structure refinement, respectively. The chemical composition of the samples was determined by M1 site refinement in single crystal structure analysis. It was assumed, that the M2 and the T sites are fully and exclusively occupied by lithium and silicon, respectively. Lattice parameters were refined at 298 K from powder X-ray diffraction data (Siemens D500, CuK_α radiation, secondary graphite monochromator) of ground single crystals, using Le-Bail whole pattern refinements as implemented in the program FULLPROF (Rodriguez-Carvajal, 2001). Data were collected between 10° and 110° 2θ, and silicon (a = 5.43094 Å at 298 K) was used as an internal standard.

Results and discussion

With the exception of $LiCrSi_2O_6$, all clinopyroxenes investigated here, show *C2/c* symmetry at room temperature (295 ± 2 K), $LiCrSi_2O_6$ has space group $P2_1/c$. At 330 K, $LiCrSi_2O_6$ transforms to the *C2/c* high-temperature structure (Redhammer, 2001; Redhammer and Roth 2004). For the sake of comparison (same space group for all compounds) the structural data for $LiCrSi_2O_6$ are those of the *C2/c* phase at a temperature of 335(1) K, well above the phase transition. For $LiScSi_2O_6$, single-crystal results from high-temperature/high-pressure experiments and from flux growth experiments are compared to each other. The structures are identical within experimental error. Thus we assume that structural variations within the Li-clinopyroxene series solely depend on different chemistries and are not affected by different preparation techniques.

Details on data collection, crystallographic and refinement parameters for selected samples are given in Table 2. Fractional atomic coordinates and equivalent isotropic atomic displacement parameters can be found in Table 3 and selected bond lengths, bond angles and polyhedral distortion parameters are listed in Table 4. The structural variations within the Li-clinopyroxene series are a consequence of the substitutions on the octahedral M1 site. The average M1–O bond length is positively correlated with the ionic radii (Fig. 2) for octahedral coordination as given by Shannon and Prewitt (1969). Except for Figure 2, all structural variations in the $LiMe^{3+}Si_2O_6$ series will be discussed in terms of the average M1–O bond lengths.

It should be recalled that $LiGaSi_2O_6$ (T_p = 286 K, Sato et al. 1997) and $LiCrSi_2O_6$ are close to the $P2_1/c \rightarrow C2/c$

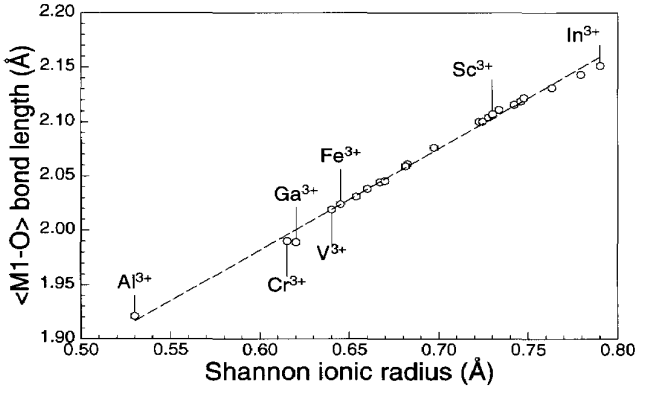

Fig. 2. Average octahedral bond lengths *vs.* the ionic radius (Shannon and Prewitt, 1969) for octahedral coordination in the $LiMe^{3+}Si_2O_6$ series. Error bars are smaller than the symbols; a linear regression line is fitted to the data as a guide to the eye.

Table 2. Experimental details for the X-ray data collection and crystallographic parameters for selected samples of the $LiMe^{3+}Si_2O_6$ series; all samples exhibit space group C2/c, $Z = 4$, absorption correction via equivalents.

	LiAl	LiGa	LiCr	LiV	LiFe	ScFe90	ScFe75	ScFe70	ScFe50
Crystal data									
T (K)	295(2)	295(2)	335(2)	295(2)	295(2)	295(2)	295(2)	295(2)	295(2)
a (Å)	9.474(4)	9.593(3)	9.570(3)	9.657(4)	9.664(2)	9.678(4)	9.686(4)	9.704(4)	9.723(3)
b (Å)	8.390(4)	8.584(2)	8.582(4)	8.623(4)	8.660(2)	8.697(2)	8.718(2)	8.737(2)	8.795(3)
c (Å)	5.219(3)	5.284(3)	5.268(2)	5.287(2)	5.293(1)	5.300(2)	5.308(2)	5.312(2)	5.322(1)
β (°)	110.07(5)	110.22(4)	110.18(4)	110.15(5)	110.19(3)	110.15(4)	110.20(4)	110.20(4)	110.25(3)
V (Å^3)	389.66	408.21	406.03	413.32	415.78	418.79	420.68	422.66	427.00
M_r	186.1	228.84	211.12	210.06	214.97	213.61	213.07	212.11	210.34
D_{calc} (g/cm^3)	3.172	3.724	3.454	3.376	3.434	3.388	3.364	3.330	3.275
μ (mm^{-1})	1.07	7.27	3.35	2.92	4.14	3.88	3.77	3.60	3.27
Colour	transparent	transparent	emerald-green	grass-green	yellow-green	yellow-green	yellow green	yellow green	pale yellow-green
shape	prism-plate	cuboid	prism	needle	prism	prism	cuboid	cuboid	prism
size max (mm)	0.21	0.15	0.16	0.11	0.15	0.14	0.15	0.16	0.14
Data collection									
$2\theta_{max}$ (°)	56.11	56.21	56.11	56.28	55.84	55.75	55.99	55.89	55.94
hkl range: h	$-12 \rightarrow 12$	$-12 \rightarrow 11$	$-12 \rightarrow 12$	$-12 \rightarrow 12$	$-12 \rightarrow 12$	$-12 \rightarrow 12$	$-12 \rightarrow 12$	$-12 \rightarrow 12$	$-12 \rightarrow 12$
k	$-9 \rightarrow 10$	$-11 \rightarrow 11$	$-11 \rightarrow 10$	$-11 \rightarrow 11$	$-11 \rightarrow 11$	$-11 \rightarrow 11$	$-11 \rightarrow 11$	$-11 \rightarrow 11$	$-11 \rightarrow 11$
l	$-6 \rightarrow 6$	$-6 \rightarrow 6$	$-6 \rightarrow 6$	$-6 \rightarrow 6$	$-6 \rightarrow 6$	$-6 \rightarrow 6$	$-6 \rightarrow 6$	$-6 \rightarrow 6$	$-6 \rightarrow 6$
$T_{min.}$	0.74	0.30	0.38	0.63	0.42	0.40	0.56	0.48	0.32
$T_{max.}$	0.92	0.43	0.67	0.68	0.60	0.51	0.60	0.56	0.49
$N_{measured}$	1857	1811	1536	1665	3173	2001	2035	2101	2335
$N_{independent}$	444	489	275	397	501	459	484	489	503
R_{int} (%)	2.86	3.80	6.77	3.52	2.84	4.39	2.29	2.51	3.41
Refinement									
$N_{parameters}$	48	48	48	47	47	49	49	49	49
$R_1 > 4\sigma$ (%)	1.88	1.82	3.85	2.33	1.49	1.76	1.63	1.67	1.94
R_1 all (%)	2.57	3.03	4.22	3.44	1.75	1.93	1.89	2.16	2.19
$wR_2 > 4\sigma$ (%)	5.24	3.63	9.27	5.39	4.95	4.90	4.26	4.41	5.82
wR_2 all (%)	5.63	3.82	10.71	5.78	5.68	6.42	5.92	7.31	7.50
G.O.F.	1.296	0.996	1.332	1.080	1.373	1.512	1.570	1.769	1.507
$\Delta\sigma_{min}$ (e/Å^3)	−0.33	−0.41	−0.67	−0.41	−0.32	−0.37	−0.43	−0.34	−0.35
$\Delta\sigma_{max}$ (e/Å^3)	0.44	0.44	0.48	0.50	0.36	0.34	0.31	0.33	0.35
weight w (a, b)	0.0400	0.0154	0.0686	0.0337	0.0296/0.381	0.0231/0.501	0.0270/0.202	0.0309	0.0395/0.044
Extinction (x)	0.0515	0.0063	0.454	–	–	–	–	–	–

$T_{min.}$ = minimum transmission, $T_{max.}$ = maximum transmission,
$R_1 = \sum ||F_o| - |F_c|| / \sum |F_o|$, $wR_2 = \{\sum [w(F_o^2 - F_c^2)^2] / \sum [w(F_o^2)^2]\}^{1/2}$, $w = 1/[\sigma^2(F_o^2) + (aP)^2 + bP]$ where $P = [2F_c^2 + \max(F_o^2, 0)]/3$,
Extinction: F_c is multiplied by the overall scale factor $k[1 + 0.001xF_c^2\lambda^3/\sin(2\Theta)]^{-1/4}$ where the extinction parameter x is refined.

phase transition. Particularly the lattice parameters change drastically in the vicinity of the phase transition. Thus, the small deviations of the Ga^{3+} and Cr^{3+} data from the linear plot for the other $LiMe^{3+}Si_2O_6$ clinopyroxenes should also be seen in the light of the closeness of the $P2_1/c \rightarrow C2/c$ phase transition.

Lattice parameters

Figure 3 depicts the changes in lattice parameters within the $LiMe^{3+}Si_2O_6$ series. The most remarkable data course is the a-lattice parameter for the $LiSc_{1-x}In_xSi_2O_6$ series. While a increases steadily from $LiAlSi_2O_6$ to $LiScSi_2O_6$, no changes are observed for the $LiSc_{1-x}In_xSi_2O_6$ series, although the smaller Sc^{3+} ($r^{VI} = 0.73$ Å) is replaced by the larger In^{3+} ($r^{VI} = 0.79$ Å, Shannon and Prewitt, 1969). Within this solid-solution series, the increase of b and c with increasing ⟨M1—O⟩ is also smaller than the changes for the other compositions. A deviation from a linear variation of lattice parameters *vs.* ⟨M1—O⟩ is evident for c and the monoclinic angle β.

The octahedral M1 site

The variations of structural parameters in the $LiMe^{3+}Si_2O_6$ clinopyroxenes are dominated by the M1 site. The ionic radius for octahedral coordination ranges between 0.53 Å for Al^{3+} and 0.79 Å for In^{3+} (Shannon and Prewitt, 1969).

Table 2. (Continued)

	ScFe40	ScFe25	ScPx	LiSc2	LiIn25	LiIn50	LiIn65	LiIn90	LiIn100
Crystal data									
T (K)	295(2)	295(2)	295(2)	295(2)	295(2)	295(2)	295(2)	295(2)	295(2)
a (Å)	9.747(3)	9.794(4)	9.805(3)	9.805(3)	9.801(3)	9.801(3)	9.802(2)	9.806(2)	9.807(2)
b (Å)	8.846(3)	8.917(2)	8.949(2)	8.949(2)	8.965(2)	8.985(2)	9.005(3)	9.035(3)	9.055(2)
c (Å)	5.335(1)	5.351(2)	5.358(2)	5.358(2)	5.361(1)	5.366(1)	5.370(1)	5.377(1)	5.383(1)
β (°)	110.28(3)	110.36(4)	110.39(3)	110.39(4)	110.38(3)	110.38(2)	110.41(3)	110.46(3)	110.49(2)
V (Å^3)	431.45	438.11	440.64	440.64	441.57	442.94	444.22	446.33	447.77
M_r	208.17	204.89	204.08	204.08	218.05	224.17	242.50	260.84	273.94
D_{calc} (g/cm^3)	3.205	3.106	3.076	3.076	3.280	3.361	3.626	3.882	4.064
μ (mm^{-1})	2.87	2.30	2.16	2.16	2.89	3.20	4.16	5.09	5.76
Colour	pale yellow	pale yellow	white transp.	white transp.	white transp.	white transp.	white transp.	white transp.	white transp.
shape	cuboid	prism	prism	prism	prism	prism	cuboid	prism	prism
size max (mm)	0.16	0.24	0.16	0.23	0.20	0.28	0.17	0.23	0.16
Data collection									
$2\theta_{max}$ (°)	55.93	56.16	55.52	56.25	56.20	55.89	56.08	56.01	55.84
hkl range: h	$-12 \rightarrow 12$	$-12 \rightarrow 12$	$-12 \rightarrow 12$	$-12 \rightarrow 12$	$-12 \rightarrow 12$	$-12 \rightarrow 12$	$-12 \rightarrow 12$	$-12 \rightarrow 12$	$-12 \rightarrow 12$
k	$-11 \rightarrow 11$	$-11 \rightarrow 11$	$-11 \rightarrow 11$	$-11 \rightarrow 11$	$-11 \rightarrow 11$	$-11 \rightarrow 11$	$-11 \rightarrow 11$	$-11 \rightarrow 11$	$-11 \rightarrow 11$
l	$-6 \rightarrow 6$	$-6 \rightarrow 6$	$-6 \rightarrow 6$	$-7 \rightarrow 7$	$-7 \rightarrow 7$	$-6 \rightarrow 7$	$-6 \rightarrow 6$	$-7 \rightarrow 7$	$-6 \rightarrow 6$
$T_{min.}$	0.62	0.58	0.58	0.59	0.45	0.42	0.52	0.35	0.37
$T_{max.}$	0.66	0.68	0.72	0.79	0.69	0.67	0.63	0.54	0.52
$N_{measured}$	2087	2122	2093	2129	2116	2268	2142	2117	2375
$N_{independent}$	487	516	522	538	533	514	495	535	500
R_{int} (%)	3.18	2.29	2.73	3.12	2.80	5.66	2.73	4.56	3.28
Refinement									
$N_{parameters}$	49	49	49	48	50	50	49	50	47
$R_1 > 4\sigma$ (%)	2.58	1.75	1.54	1.94	2.08	2.88	1.38	1.66	1.39
R_1 all (%)	3.15	1.98	1.87	2.40	2.32	3.25	1.64	1.98	1.70
$wR_2 > 4\sigma$ (%)	6.52	4.66	4.23	5.22	5.18	6.78	3.26	4.17	3.61
wR_2 all (%)	7.71	7.26	5.54	6.29	6.36	7.13	3.52	4.90	3.66
G.O.F.	1.228	1.715	1.470	1.318	1.411	1.810	1.268	1.384	1.106
$\Delta\sigma_{min}$ (e/Å^3)	−0.51	−0.29	−0.24	−0.31	−0.61	−0.86	−0.26	−0.97	−0.85
$\Delta\sigma_{max}$ (e/Å^3)	0.44	0.33	0.30	0.47	0.45	1.03	0.29	0.54	0.44
weight w (a, b)	0.0473	0.0352/0.015	0.0236/0.316	0.0342/0.053	0.0365/0.059	0.0210/0.989	0.0138/0.566	0.0217	0.0213/0.355
Extinction (x)	–	–	0.0198	0.0647	0.0261	0.0173	–	0.0029	–

see above

The substitution of cations larger than In^{3+} (e.g. Y^{3+}) was not possible. The edge-sharing zig-zag chain of M1 sites represents a very robust unit. Changes within it force rearrangements in the (average) geometry of the corner-sharing tetrahedral chain and within the M2–O polyhedra.

The variation of individual M1–O bond lengths *vs.* ionic radius (Fig. 4a) is not uniform. The most pronounced increase is observed for the four M1–O bonds within the equatorial plane of the octahedron, the M1–O1(a2, b2) bonds to the apex oxygen atoms exhibit a smaller increase. With increasing size of the large cation, the octahedra become more and more tetragonally compressed. This is also expressed by O1(a2)–M1–O1(b2) bond angles, which linearly decrease from 174.7(1)° in $LiAlSi_2O_6$ to 168.1(1)° in $LiInSi_2O_6$, except for Cr^{3+} and V^{3+} samples (Table 4). The latter two have shorter M1–O1(a1, b1), somewhat longer M1–O2(c1, d1) bonds and more ideal, i.e. closer to 180°, O1(a2)–M1–O1(b2) and O1–M1–O2 bond angles. Thus the octahedra in these two compounds appear to be more regular in terms of the octahedral angle variance (OAV[1], Renner and Lehmann, 1986) and are distinctly different from the overall trend observed for the other samples (Fig. 4b). The very similar behaviour has been described very recently by

[1] $OAV = \sum_{i=1}^{12} (\Theta_i - 90°)^2/11$ with Θ_i = O–M–O bonding angle (Renner and Lehmann, 1986).

Table 3. Atomic coordinates and equivalent isotropic displacement parameters for selected samples of the $LiMe^{3+}Si_2O_6$ series.

		LiAl	LiGa	LiCr	LiV	LiFe(1)	ScFe90	ScFe75	ScFe70	ScFe50
M2 (Li)	x	0.0	0.0	0.0	0.0	0.0	0.0	0.0	0.0	0.0
	y	0.2746(4)	0.2654(9)	0.2656(9)	0.2678(8)	0.2628(5)	0.2605(5)	0.2601(5)	0.2600(5)	0.2586(6)
	z	1/4	1/4	1/4	1/4	1/4	1/4	1/4	1/4	1/4
	U_{eq}	0.0154(7)	0.0148(16)	0.0235(16)	0.0124(12)	0.0143(8)	0.0182(9)	0.0181(8)	0.0190(9)	0.0192(10)
M1	x	0.0	0.0	0.0	0.0	0.0	0.0	0.0	0.0	0.0
	y	0.90674(7)	0.90159(6)	0.90861(6)	0.90589(7)	0.89835/3)	0.89809(3)	0.89785(3)	0.89764(3)	0.89696(4)
	z	1/4	1/4	1/4	1/4	1/4	1/4	1/4	1/4	1/4
	U_{eq}	0.0035(2)	0.0023(1)	0.0094(3)	0.0023(1)	0.0035(1)	0.0040(1)	0.0040(1)	0.0038(1)	0.0049(2)
	Occ.	1.00 Al	1.00 Ga	1.00 Cr	1.00 V	1.00 Fe	0.127(3) Fe	0.177(6) Fe	0.261(6) Fe	0.426(7) Fe
	Occ.	–	–	–	–	–	0.873(3) Sc	0.826(6) Sc	0.739(6) Sc	0.573(7) Sc
T (Si)	x	0.29413(3)	0.29654(6)	0.29812(9)	0.29678(6)	0.29611(5)	0.29646(5)	0.29663(4)	0.29677(4)	0.29733(5)
	y	0.09354(4)	0.09102(9)	0.09152(7)	0.09058(8)	0.08949(5)	0.08933(4)	0.08916(8)	0.08900(4)	0.08848(5)
	z	0.25599(7)	0.2610(1)	0.2619(2)	0.2685(1)	0.26580(8)	0.26642(9)	0.26702(8)	0.26763(9)	0.26976(10)
	U_{eq}	0.0032(1)	0.0020(2)	0.0099(3)	0.0024(2)	0.0033(1)	0.0045(1)	0.0044(1)	0.0045(2)	0.0058(2)
O1	x	0.1096(1)	0.1135(2)	0.1153(2)	0.1170(2)	0.1160(1)	0.1162(1)	0.1166(1)	0.1171(1)	0.1180(1)
	y	0.0825(1)	0.0838(2)	0.0846(2)	0.0858(2)	0.0846(1)	0.0846(1)	0.0846(1)	0.0845(1)	0.0844(1)
	z	0.1404(2)	0.1441(3)	0.1474(5)	0.1553(4)	0.1497(2)	0.1499(2)	0.1505(2)	0.1507(2)	0.1520(3)
	U_{eq}	0.0044(2)	0.0037(4)	0.0109(6)	0.0038(4)	0.0046(2)	0.0059(3)	0.0059(2)	0.0062(3)	0.0072(3)
O2	x	0.3647(1)	0.3653(2)	0.3676(2)	0.3689(2)	0.3662(1)	0.3667(1)	0.3671(1)	0.3673(1)	0.3681(1)
	y	0.2669(1)	0.2617(2)	0.2616(3)	0.2599(2)	0.2584(1)	0.2578(1)	0.2572(1)	0.2565(1)	0.2547(1)
	z	0.3004(2)	0.3241(4)	0.3241(4)	0.3273(4)	0.3252(2)	0.3267(3)	0.3281(3)	0.3294(3)	0.3333(3)
	U_{eq}	0.0073(2)	0.0073(4)	0.0150(5)	0.0072(4)	0.0081(2)	0.0097(3)	0.0097(2)	0.0099(3)	0.0113(3)
O3	x	0.35650(9)	0.3568(2)	0.3573(2)	0.3557(2)	0.3557(1)	0.3558(1)	0.3556(1)	0.3554(1)	0.3554(1)
	y	−0.0133(1)	−0.0003(2)	−0.0012(2)	−0.0023(3)	−0.0013(1)	−0.0010(1)	−0.0002(1)	0.0066(1)	0.0021(2)
	z	0.0585(2)	0.0497(3)	0.0513(5)	0.0568(3)	0.0553(2)	0.0550(3)	0.0549(3)	0.0548(3)	0.0547(3)
	U_{eq}	0.0069(2)	0.0064(4)	0.0165(5)	0.0077(4)	0.0084(2)	0.0105(3)	0.0105(3)	0.0108(3)	0.0121(3)

		ScFe40	ScFe25	ScPx	LiSc2	LiIn25	LiIn50	LiIn65	LiIn90	LiIn100
M2 (Li)	x	0.0	0.0	0.0	0.0	0.0	0.0	0.0	0.0	0.0
	y	0.2571(7)	0.2566(4)	0.2567(4)	0.2568(6)	0.2545(6)	0.2533(9)	0.2523(6)	0.2501(8)	0.2492(7)
	z	1/4	1/4	1/4	1/4	1/4	1/4	1/4	1/4	1/4
	U_{eq}	0.0209(13)	0.0192(7)	0.0180(8)	0.0170(9)	0.0181(9)	0.0180(15)	0.0181(12)	0.0164	0.0132(14)
M1	x	0.0	0.0	0.0	0.0	0.0	0.0	0.0	0.0	0.0
	y	0.89631(5)	0.89523(3)	0.89509(3)	0.89502(5)	0.89436(3)	0.89401(4)	0.89341(3)	0.89288(3)	0.89257
	z	1/4	1/4	1/4	1/4	1/4	1/4	1/4	1/4	1/4
	U_{eq}	0.0075(2)	0.0046(1)	0.0030(1)	0.0033(2)	0.00308	0.0037(2)	0.0032(1)	0.0028(1)	0.0016(1)
		0.385(4) Fe	0.087(3) Fe	–	–	0.203 (3) In	0.289(2) In	0.553(2) In	0.815(3) In	1.00 In
		0.614(4) Sc	0.913(3) Sc	1.00 Sc	1.00 Sc	0.787 (3) Sc	0.710 (2) Sc	0.447(2) Sc	0.185(3) Sc	–
T (Si)	x	0.29783(6)	0.29873(3)	0.29888(3)	0.29885(5)	0.29959(5)	0.29983(7)	0.30044(5)	0.30114(6)	0.30125(6)
	y	0.08790(6)	0.08703(4)	0.08677(4)	0.08687(5)	0.08650(5)	0.08636(8)	0.08581(5)	0.08114(8)	0.08513(7)
	z	0.2721(1)	0.27668(7)	0.27774(7)	0.27779(8)	0.27812(9)	0.2782(1)	0.2786(1)	0.2794(1)	0.2795(2)
	U_{eq}	0.0083(2)	0.0046(1)	0.0029(1)	0.0033(2)	0.0038(1)	0.0049(2)	0.0039(1)	0.0039(2)	0.0017(1)
O1	x	0.1189(2)	0.12042(8)	0.12081(9)	0.1208(1)	0.12114(1)	0.1215(2)	0.1221(1)	0.1223(2)	0.1225(2)
	y	0.0842(2)	0.08370(8)	0.08338(9)	0.0834(1)	0.0832(1)	0.0833(2)	0.0832(1)	0.0828(2)	0.0829(2)
	z	0.1541(4)	0.1572(2)	0.1578(2)	0.1580(2)	0.1590(2)	0.1596(4)	0.1606(3)	0.1618(4)	0.1627(4)
	U_{eq}	0.0097(4)	0.0060(2)	0.0044(2)	0.0044(3)	0.0054(3)	0.0058(4)	0.0054(3)	0.0053(4)	0.0034(4)
O2	x	0.3687(2)	0.37025(8)	0.3706(1)	0.3705(1)	0.3709(1)	0.3711(2)	0.3715(1)	0.3716(2)	0.3716(2)
	y	0.2526(2)	0.24952(9)	0.2490(1)	0.2490(1)	0.2478(1)	0.2472(2)	0.2465(2)	0.2453(2)	0.2444(2)
	z	0.3371(4)	0.3432(2)	0.3445(2)	0.3446(2)	0.3494(2)	0.3518(4)	0.3566(3)	0.3616(3)	0.3639(4)
	U_{eq}	0.0136(4)	0.0096(2)	0.0078(2)	0.0079(3)	0.0088(2)	0.0097(4)	0.0092(3)	0.0080(4)	0.0056(4)
O3	x	0.3549(2)	0.35470(8)	0.35442(9)	0.3544(1)	0.3545(1)	0.3545(2)	0.3544(1)	0.3542(2)	0.3541(2)
	y	0.0032(2)	0.0053(1)	0.0054(1)	0.0054(2)	0.0088(2)	0.0096(2)	0.0126(2)	0.0150(2)	0.0165(2)
	z	0.0553(4)	0.0570(2)	0.0575(2)	0.0574(3)	0.0547(3)	0.0533(4)	0.0504(3)	0.0479(3)	0.0479(4)
	U_{eq}	0.0152(4)	0.0109(2)	0.0093(2)	0.0096(3)	0.0102(3)	0.0116(4)	0.0096(3)	0.0085(7)	0.0060(4)

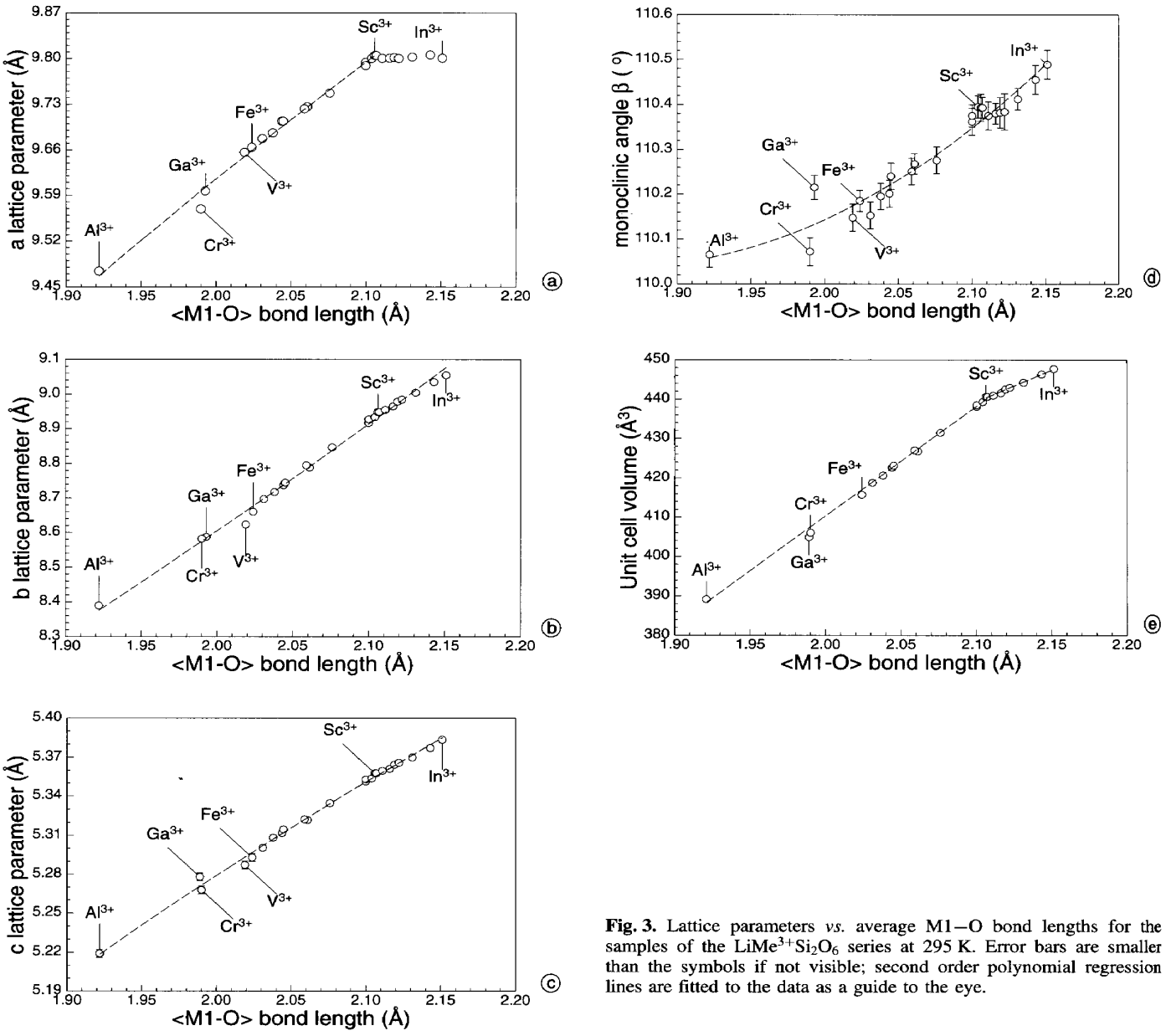

Fig. 3. Lattice parameters *vs.* average M1—O bond lengths for the samples of the $LiMe^{3+}Si_2O_6$ series at 295 K. Error bars are smaller than the symbols if not visible; second order polynomial regression lines are fitted to the data as a guide to the eye.

Redhammer, Ohashi and Roth (2003) for the $NaM^{3+}Si_2O_6$ series. When plotting the OAV *vs.* the average M1—O bond lengths (or the M1 ionic radius) for the $NaM^{3+}Si_2O_6$ series, compounds with M^{3+} = Cr, V, Mn and Ti significantly deviate from the trend defined by the Al—Ga—Fe—Sc samples. The deviation of individual bond lengths from their average value (BLD[2], Renner and Lehmann, 1986) is rather large but typical for the Li-clinopyroxenes and amounts to 3.4% in $LiAlSi_2O_6$. The BLD (Fig. 4c) steadily decreases — with a discontinuity at $LiFeSi_2O_6$ — towards $LiInSi_2O_6$ (2.3%). This discontinuity might be associated with the transition from the "S" to the "O" conformation of the tetrahedral chains.

As noted above, $LiCrSi_2O_6$ and $LiVSi_2O_6$ deviate from the Al—Ga—Fe—Sc series. This also is evident, when plotting e.g. the average M1—O1 bond lengths *vs.* the M1—M1 interatomic distance or *vs.* the O1—M1—O1 bond angles (Fig 4d). Data for $LiTiSi_2O_6$ (Redhammer, Ohashi, Roth, preliminary results; Kopnin, Sato and Takayama-Muromachi, 2003) are included in Fig. 4d. As the O1—M1—O1 bond angles are closer to the ideal values of 90° and 180° respectively (Table 4, Fig. 4d) this is one reason for the smaller OAV in the Cr^{3+} and V^{3+} compound. The deviation of the Cr^{3+}, V^{3+} (and Ti^{3+}) composition from the other members of the $LiM^{3+}Si_2O_6$ series may be caused by the repulsion between the O1 atoms and the unpaired 3d electrons of the above mentioned transition metal ions. Ohashi, Osawa and Tsukimura (1987) and later on Redhammer et al. (2003) noted that the geometry of the M1 site can also be characterized by plotting the M1—M1 interatomic distance *vs.* the mean

[2] $\mathrm{BLD} = \frac{100}{n} \sum_{i=1}^{n} \frac{|(\mathrm{X-O})_i - (\langle \mathrm{X-O} \rangle)|}{(\langle \mathrm{X-O} \rangle)}$ %, n = amount of cation-anion bonds and X—O = cation-anion (oxygen) distance (Renner and Lehmann, 1986).

Table 4. Selected bond distances (Å) and angles (°) and polyhedral distortion parameters for selected samples of the $LiMe^{3+}Si_2O_6$ series.

Sample/ Temperature (K)	LiAl 298	LiGa 298	LiCr 336	LiV 298	LiFe 298	ScFe90 298	ScFe75 298	ScFe70 298	ScFe50 298
M2–O2	2.282(2)	2.181(2)	2.176(2)	2.169(2)	2.178(1)	2.175(2)	2.169(3)	2.164(2)	2.147(2)
M2–O1	2.100(3)	2.078(6)	2.081(6)	2.093(6)	2.077(4)	2.073(4)	2.076(4)	2.082(4)	2.085(4)
M2–O3	2.254(2)	2.469(6)	2.445(6)	2.436(6)	2.492(4)	2.515(4)	2.529(4)	2.539(4)	2.575(4)
⟨M2–O⟩	*2.212*	*2.243*	*2.234*	*2.233*	*2.249*	*2.254*	*2.258*	*2.262*	*2.269*
BLD [%]	3.4(1)	6.7(1)	6.3(1)	6.1(1)	7.2(1)	7.7(1)	8.0(1)	8.2(1)	9.0(1)
M1–O2	1.822(1)	1.897(2)	1.919(2)	1.926(2)	1.910(1)	1.918(1)	1.924(1)	1.932	1.950
M1–O1	1.946(1)	1.992(2)	2.002(3)	2.051(2)	2.028(1)	2.034(1)	2.040(1)	2.043	2.054
M1–O1	1.997(1)	2.091(2)	2.050(2)	2.079(2)	2.135(1)	2.142(1)	2.149(1)	2.156	2.173
⟨M1–O⟩	*1.922*	*1.993*	*1.990*	*2.019*	*2.024*	*2.031*	*2.038*	*2.044*	*2.059*
BLD (%)	3.5(1)	3.3(1)	2.4(1)	3.1(1)	3.8(1)	3.7(1)	3.7(1)	3.7(1)	3.7(1)
⟨O–O⟩	*2.714*	*2.810*	*2.812*	*2.850*	*2.853*	*2.862*	*2.871*	*2.879*	*2.901*
$\langle O-O\rangle_s = e_s$	*2.623*	*2.698*	*2.708*	*2.751*	*2.747*	*2.756*	*2.763*	*2.771*	*2.789*
$\langle O-O\rangle_u = e_u$	*2.778*	*2.890*	*2.886*	*2.920*	*2.928*	*2.939*	*2.949*	*2.957*	*2.981*
e_u/e_s	1.059	1.071	1.066	1.062	1.066	1.066	1.067	1.067	1.069
ELD (%)	3.4(1)	3.8(1)	3.5(1)	3.3(1)	3.3(1)	3.3(1)	3.3(1)	3.3(1)	3.2(1)
M1–M1 (intra)	3.043(1)	3.129(1)	3.065(1)	3.102(1)	3.179(1)	3.188(1)	3.196(1)	3.202(1)	3.220(1)
M1–M1 (inter)	5.254(1)	5.273(1)	5.343(1)	5.287(1)	5.304(1)	5.314(1)	5.317(1)	5.325(1)	5.333(1)
O1–M1–O1	84.8(1)	83.2(1)	85.1(1)	83.5(1)	81.7(1)	81.6(1)	81.5(1)	81.5(1)	81.3(1)
O1–M1–O1 ×2	79.0(1)	79.8(1)	81.7(1)	82.6(1)	80.5(1)	80.5(1)	80.6(1)	80.7(1)	80.8(1)
O1–M1–O1 ×2	97.0(1)	94.8(1)	95.8(1)	94.4(1)	93.3(1)	93.1(1)	92.9(1)	92.7(1)	92.2(1)
O1–M1–O1	174.7(1)	172.7(1)	176.7(1)	176.0(1)	171.8(1)	171.5(1)	171.4(1)	171.3(1)	170.9(1)
O1–M1–O2 ×2	88.5(1)	87.9(1)	88.3(1)	88.1(1)	88.7(1)	88.9(1)	89.0(1)	89.0(1)	89.3(1)
O1–M1–O2 ×2	91.6(1)	89.5(1)	88.7(1)	89.1(1)	89.9(1)	89.8(1)	89.7(1)	89.7(1)	89.5(1)
O1–M1–O2 ×2	91.8(1)	95.1(1)	93.9(1)	94.5(1)	95.4(1)	95.6(1)	95.8(1)	95.9(1)	96.5(1)
O1–M1–O2 ×2	167.8(1)	169.2(1)	171.9(1)	171.9(1)	169.2(1)	169.4(1)	169.6(1)	169.8(1)	170.1(1)
O2–M1–O2	99.9(1)	101.7(1)	97.9(1)	98.4(1)	101.3(1)	101.0(1)	100.8(1)	100.7(1)	100.2(1)
OAV [°]	50.6(5)	51.5(5)	31.4(5)	30.1(5)	49.7(5)	49.3(5)	49.0(5)	48.3(5)	48.2(5)
Si–O2	1.585(1)	1.594(1)	1.590(2)	1.602(2)	1.599(1)	1.601(1)	1.601(1)	1.601(1)	1.601(1)
Si–O3	1.622(1)	1.624(1)	1.618(2)	1.622(2)	1.624(1)	1.627(1)	1.626(2)	1.627(1)	1.629(1)
Si–O3	1.630(1)	1.628(1)	1.628(2)	1.630(2)	1.628(1)	1.629(1)	1.631(2)	1.631(1)	1.631(1)
Si–O1	1.644(1)	1.647(1)	1.643(2)	1.630(2)	1.636(1)	1.638(1)	1.637(1)	1.637(1)	1.637(1)
⟨Si–O⟩	*1.620*	*1.623*	*1.620*	*1.621*	*1.622*	*1.624*	*1.624*	*1.624*	*1.625*
BLD [%]	1.1(1)	0.901(1)	0.972(1)	0.586(1)	0.701(1)	0.701(1)	0.701(1)	0.708(1)	0.723(1)
O1c1–Si–O3c1	108.0(1)	108.5(1)	108.1(1)	108.4(1)	108.9(1)	109.1(1)	109.0(1)	109.0(1)	109.0(1)
O1c1–Si–O3c2	108.6(1)	108.1(1)	108.0(1)	108.5(1)	108.3(1)	108.1(1)	108.0(1)	107.9(1)	107.6(1)
O1c1–Si–O2c1	116.6(1)	115.2(1)	115.1(1)	115.6(1)	114.9(1)	115.0(1)	115.0(1)	115.1(1)	115.1(1)
O2c1–Si–O3c1	111.9(1)	111.5(1)	111.9(1)	110.5(1)	110.5(1)	110.7(1)	110.6(1)	110.5(1)	110.3(1)
O2c1–Si–O3c2	104.1(1)	104.9(1)	105.0(1)	104.9(1)	104.9(1)	104.9(1)	105.0(1)	105.1(1)	105.3(1)
O3c1–Si–O3c2	107.3(1)	108.5(1)	108.5(1)	108.8(1)	109.1(1)	109.0(1)	109.2(1)	109.2(1)	109.5(1)
TAV [°]^2	18.6(5)	12.4(5)	12.6(5)	12.3(5)	10.8(5)	11.1(5)	10.9(5)	10.9(5)	10.5(5)
τ	111.1(1)	110.6(1)	110.4(1)	110.8(1)	110.7(1)	110.7(1)	110.7(1)	110.6(1)	110.6(1)
O3–O3–O3	170.3(1)	179.9(1)	179.0(1)	178.3(1)	179.2(1)	179.2(1)	179.8(1)	179.8(1)	178.4(1)

$\text{BLD} = \frac{100}{n}\sum_{i=1}^{n}\frac{|(\text{X}-\text{O})_i - (\langle\text{X}-\text{O}\rangle)|}{(\langle\text{X}-\text{O}\rangle)}$ %, n = amount of cation-anion bonds and X–O = cation-anion (oxygen) distance (Renner and Lehmann, 1986);

$\text{ELD} = \frac{100}{n}\sum_{i=1}^{n}\frac{|(\text{O}-\text{O})_i - (\langle\text{O}-\text{O}\rangle)|}{(\langle\text{O}-\text{O}\rangle)}$ %, n = amount of edges and (O–O) = oxygen-oxygen interatomic distance defining an edge of the octahedron;

e_u/e_s = mean of the O–O interatomic distances defining unshared edges of the octahedron (e_u)/mean of the O–O interatomic distances defining the shared edges of the octahedron (e_s), Toraya (1981);

Table 4. (Continued)

Sample/ Temperature/ K	ScFe40 298	ScFe25 298	ScPx 298	LiSc2 298	LiIn25 298	LiIn50 298	LiIn65 298	LiIn90 298	LiIn100 298
M2–O2	2.132(2)	2.105(1)	2.100(1)	2.100(2)	2.079(2)	2.069(2)	2.048(2)	2.027(2)	2.018(2)
M2–O1	2.087(5)	2.103(3)	2.112(3)	2.113(4)	2.102(4)	2.095(6)	2.094(4)	2.084(6)	2.080(5)
M2–O3	2.608(5)	2.645(3)	2.651(3)	2.651(4)	2.699(4)	2.720(6)	2.759(4)	2.805(6)	2.828(5)
$\langle M2–O\rangle$	*2.276*	*2.284*	*2.288*	*2.288*	*2.293*	*2.295*	*2.300*	*2.305*	*2.309*
BLD [%]	9.7(1)	10.5(1)	10.6(1)	10.6(1)	11.8(1)	12.4(1)	13.3(1)	14.4(1)	15.0(1)
M1–O2	1.971(2)	1.998(1)	2.006(1)	2.007(1)	2.021(1)	2.029(2)	2.041(1)	2.062(2)	2.075(2)
M1–O1	2.071(2)	2.094(1)	2.100(1)	2.101(2)	2.109(1)	2.113(2)	2.121(2)	2.129(2)	2.135(2)
M1–O1	2.186(2)	2.207(1)	2.212(1)	2.212(1)	2.219(1)	2.225(2)	2.232(1)	2.237(2)	2.243(2)
$\langle M1–O\rangle$	*2.076*	*2.100*	*2.106*	*2.107*	*2.116*	*2.122*	*2.131*	*2.143*	*2.151*
BLD [%]	3.5(1)	3.4(1)	3.4(1)	3.3(1)	3.2(1)	3.2(1)	3.2(1)	2.9(1)	2.9(1)
$\langle O–O\rangle$	*2.925*	*2.958*	*2.967*	*2.968*	*2.980*	*2.989*	*3.001*	*3.016*	*3.027*
$\langle O–O\rangle_s = e_s$	*2.809*	*2.837*	*2.845*	*2.845*	*2.851*	*2.854*	*2.860*	*2.864*	*2.870*
$\langle O–O\rangle_u = e_u$	3.008	3.044	3.054	3.055	3.073	3.085	3.102	3.125	3.140
e_u/e_s	1.071	1.073	1.074	1.074	1.078	1.081	1.084	1.091	1.094
ELD [%]	3.3(1)	3.4(1)	3.4(1)	3.4(1)	3.6(1)	3.8(1)	3.9(1)	4.2(1)	4.3(1)
Fe-Fe (intra)	3.237(1)	3.263(1)	3.271(1)	3.272(1)	3.282(1)	3.290(1)	3.306(1)	3.313(1)	3.321(1)
Fe-Fe (inter)	5.344(1)	5.360(1)	5.367(1)	5.366(1)	5.362(1)	5.362(1)	5.360(1)	5.359(1)	5.359(1)
O1–M1–O1	81.0(1)	80.8(1)	80.8(1)	80.7(1)	80.6(1)	80.3(1)	80.1(1)	79.8(1)	79.6(1)
O1–M1–O1 ×2	81.0(1)	81.3(1)	81.4(1)	81.4(1)	81.4(1)	81.4(1)	81.4(1)	81.4(1)	81.4(1)
O1–M1–O1 ×2	91.7(1)	90.8(1)	90.6(1)	90.6(1)	90.3(1)	90.1(1)	89.8(1)	89.6(1)	89.5(1)
O1–M1–O1	170.4(1)	169.7(1)	169.5(1)	169.4(1)	169.0(1)	168.9(1)	168.6(1)	168.2(1)	168.1(1)
O1–M1–O2 ×2	89.0(1)	88.6(1)	88.5(1)	88.5(1)	88.1(1)	87.8(1)	87.3(1)	86.7(1)	86.5(1)
O1–M1–O2 ×2	89.7(1)	90.2(1)	90.3(1)	90.3(1)	90.3(1)	90.4(1)	90.4(1)	90.4(1)	90.6(1)
O1–M1–O2 ×2	97.1(1)	98.1(1)	98.4(1)	98.4(1)	99.1(1)	99.5(1)	100.2(1)	101.0(1)	101.3(1)
O1–M1–O2 ×2	170.5(1)	170.9(1)	171.1(1)	171.0(1)	170.9(1)	170.7(1)	170.4(1)	170.0(1)	169.8(1)
O2–M1–O2	99.6(1)	98.9(1)	98.6(1)	98.7(1)	98.8(1)	98.9(1)	99.2(1)	99.4(1)	99.4(1)
OAV [°]	48.2(5)	49.2(5)	49.6(5)	50.0(5)	53.3(5)	55.5(5)	59.6(5)	65.0(5)	67.3(5)
Si–O2	1.598(2)	1.595(1)	1.598(1)	1.597(1)	1.593(2)	1.593(2)	1.597(2)	1.596(2)	1.594(2)
Si–O3	1.629(2)	1.630(1)	1.629(1)	1.629(1)	1.630(2)	1.630(2)	1.630(2)	1.629(2)	1.632(2)
Si–O3	1.631(2)	1.631(1)	1.633(1)	1.634(1)	1.632(2)	1.634(2)	1.633(2)	1.637(2)	1.636(2)
Si–O1	1.636(2)	1.638(1)	1.637(1)	1.637(1)	1.638(2)	1.639(2)	1.639(2)	1.643(2)	1.642(2)
$\langle Si–O\rangle$	*1.624*	*1.624*	*1.624*	*1.624*	*1.623*	*1.624*	*1.625*	*1.626*	*1.626*
BLD [%]	0.8(1)	0.9(1)	0.8(1)	0.8(1)	0.9(1)	0.9(1)	0.9(1)	0.9(1)	1.0(1)
O1c1–Si–O3c1	108.8(1)	108.8(1)	108.7(1)	108.6(1)	108.3(1)	108.2(1)	107.9(1)	107.5(1)	107.3(1)
O1c1–Si–O3c2	107.4(1)	106.9(1)	106.7(1)	106.6(1)	106.6(1)	106.6(1)	106.5(1)	106.4(1)	106.5(1)
O1c1–Si–O2c1	115.1(1)	115.4(1)	115.5(1)	115.5(1)	115.4(1)	115.3(1)	115.1(1)	114.9(1)	114.7(1)
O2c1–Si–O3c1	110.2(1)	109.6(1)	109.6(1)	109.6(1)	109.6(1)	109.7(1)	109.7(1)	109.9(1)	109.9(1)
O2c1–Si–O3c2	105.5(1)	105.8(1)	105.9(1)	105.9(1)	106.2(1)	106.1(1)	106.4(1)	106.4(1)	106.6(1)
O3c1–Si–O3c2	109.9(1)	110.4(1)	110.5(1)	110.5(1)	110.8(1)	110.9(1)	111.3(1)	111.7(1)	111.9(1)
TAV [°]^2	10.7(5)	11.4(5)	11.7(5)	11.8(5)	11.5(5)	11.4(5)	11.0(5)	11.5(5)	11.1(5)
τ	110.4(1)	110.4(1)	110.3(1)	110.3(1)	110.1(1)	110.1(1)	109.3(1)	109.6(1)	109.5(1)
O3–O3–O3	177.6(1)	176.0(1)	175.9(1)	175.9(1)	173.3(1)	172.6(1)	170.3(1)	168.5(1)	167.4(1)

OAV $= \sum_{i=1}^{12} (\Theta_i - 90°)^2/11$ with Θ_i = O–M–O bonding angle (Renner and Lehmann, 1986);

TAV $= \sum_{i=1}^{6} (\Theta_i - 109.57°)^2/5$ with Θ_i = O–T–O bonding angle (Renner and Lehmann, 1986).

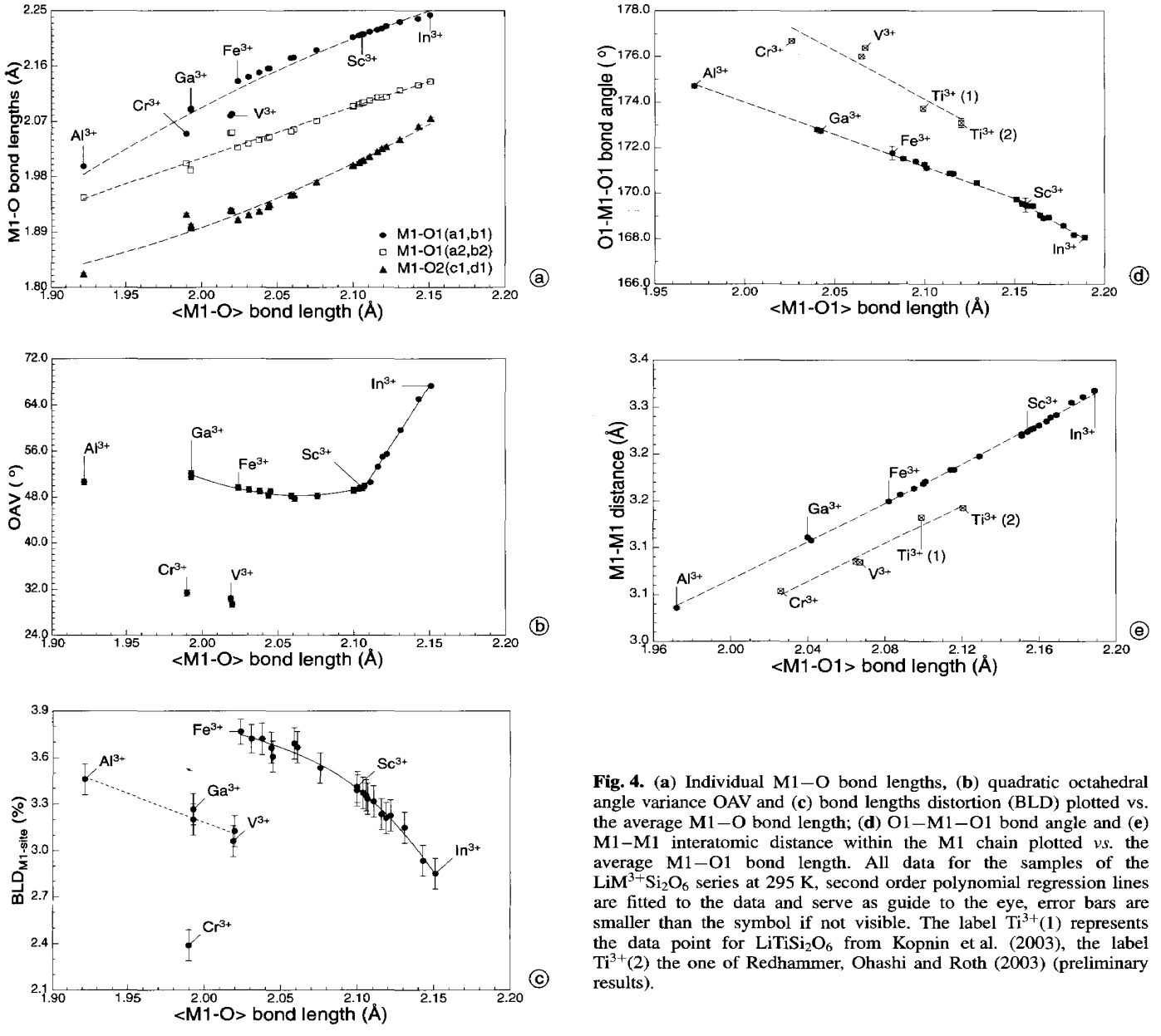

Fig. 4. (**a**) Individual M1—O bond lengths, (**b**) quadratic octahedral angle variance OAV and (**c**) bond lengths distortion (BLD) plotted vs. the average M1—O bond length; (**d**) O1—M1—O1 bond angle and (**e**) M1—M1 interatomic distance within the M1 chain plotted *vs.* the average M1—O1 bond length. All data for the samples of the $LiM^{3+}Si_2O_6$ series at 295 K, second order polynomial regression lines are fitted to the data and serve as guide to the eye, error bars are smaller than the symbol if not visible. The label $Ti^{3+}(1)$ represents the data point for $LiTiSi_2O_6$ from Kopnin et al. (2003), the label $Ti^{3+}(2)$ the one of Redhammer, Ohashi and Roth (2003) (preliminary results).

M1—O1 bond lengths. The latter two bonds are the ones, pointing form the M1 cation to the two O1 oxygen atoms, forming the common edge between two neighbouring octahedra. As can be seen from Figure 4e the data points for compounds having spherical M1 cations [Al^{3+}, Ga^{3+} ($3d^0$), Fe^{3+} ($3d^5$), Sc^{3+} ($3d^{10}$), In^{3+}] form a common, almost linear trend. The data for Cr^{3+} ($3d^3$), V^{3+} ($3d^2$) and Ti^{3+} ($3d^1$; preliminary results), with a non-spherical electron configuration distinctly fall of this trend. This shows that besides pure geometric considerations electronic effects also play an important role in defining the distortional state of the M1 octahedron.

If the M1 site is occupied by a small cation (e.g. Al^{3+}), the octahedral chain appears to be "shorter" than the tetrahedral one. In $LiAlSi_2O_6$, the M1—M1 distance is 3.043(2) Å only, in $LiCrSi_2O_6$ it is 3.065(2) Å. The cation-cation repulsion perpendicular to the O1(a2)—O1(b1) edge, which is common to two neighbouring octahedra, causes the two trivalent cations to move to the largest possible distance from each other and also out of the centres of the octahedra. The M1—O1(a1, b1) bond lengths in the equatorial plane become longer, the M1—O2(c1, d1) bond length shortens as compared to an octahedron with the cation in the centre of the anion-polyhedron. This displacement of the M1 cation has also been observed in the hedenbergite-aegirine $CaFe^{2+}Si_2O_6$—$NaFe^{3+}Si_2O_6$ solid solution series (Redhammer, 2001), where divalent iron is replaced by trivalent iron. The octahedra are stretched in chain direction, as can be seen from the rather large M1—O1(a2, b2) bond lengths. This enables the octahedral chain to fit to the tetrahedral chain. Li-clinopyroxenes having small cations on the M1 site show large M1—M1—M1 bond angles, e.g. 118.1(1)° in $LiAlSi_2O_6$, 114.7(1)° in $LiGaSi_2O_6$ as compared to 108.3(1)° in $LiInSi_2O_6$.

Increasing the size of the octahedral cation decreases the kinking of the tetrahedral chain, which shows a max-

imum elongation in c direction at 295 K in the compounds $LiGaSi_2O_6$ and $LiFeSi_2O_6$. Here the tetrahedral chains are fully expanded showing tetrahedral kinking-angles O3—O3—O3 very close to 180°. If the octahedra are expanded further by the substitution of even larger cations (Sc^{3+}, In^{3+}) into M1, the tetrahedral chain starts to hamper the expansion of the M1 chain in c direction. This explains the reduced increase of the M1—O1(a2, b2) bond lengths (Fig 4a) with increasing size of the octahedral cation. The O1(a2, b2) oxygen atom forms the common corner of the M1-octahedron and the SiO_4-tetrahedron and therefore constitutes the link between the two building units.

The substitution of larger cations on M1 is also reflected in the oxygen-oxygen interatomic distances. For most of the compounds, the average values for the unshared O—O distances (Fig. 5a) show a nearly linear correlation with the ionic radius of the octahedral cation. A similar behaviour is found for the average values of the shared O—O distances. However, the data for the $Li(Sc_{1-x}In_x)Si_2O_6$ series show a distinctly different slope for the average of the shared edges. The average of all O—O distances also reflects this different slope of the $Li(Sc_{1-x}In_x)Si_2O_6$ series. The variation of individual O—O interatomic distances is not uniform. The O1(a1)—O2(c1) distance (unshared edge, Fig. 5b), which runs along the b-axis within the equatorial plane of the octahedron, shows the largest change between $LiAlSi_2O_6$ and $LiInSi_2O_6$ and increases by 16.8%. Large changes of 13.1% and 11.8% take place for the O1(a1)—O1(c1) and the O2(c1)—O2(d1) edge. All of them are unshared edges. The smallest increase is observed for the O1(a1)—O1(a2) edge, which changes by only 4.2%. Within the $Li(Sc_{1-x}In_x)Si_2O_6$ series this distance stays constant. The oxygen atoms O1(a1) and O1(a2) form two corners of the octahedron and at the same time the apex of two corner sharing tetrahedra. Thus the O1(a1)—O1(a2) octahedral edge is hampered in its expansion due to the connection with the tetrahedral chain.

The O1(a1)—O1(b1) and the O1(a2)—O2(d1) octahedral edges (shared edges), which are common to the M1 site and the M2 polyhedron (Fig. 5c) also show small geometrical expansions of 6.6 and 6.9% within the series from the Al^{3+} and the In^{3+} compound. Within the $LiSc_{1-x}In_xSi_2O_6$ series these edge lengths stay nearly constant. The O1(a2)—O1(b1) edge, which is common to two octahedra, increases with the size of the M1 cation, however the expansion of this octahedral edge is also reduced within the $LiSc_{1-x}In_xSi_2O_6$ series. Similar to the small increase of the O1(a1)—O1(a2) edge lengths (Fig. 5b) this reduced increase is presumably related to the hampering influence of the tetrahedral chain. For $LiInSi_2O_6$ the three different shared octahedral edge lengths are similar. This is not the case for the Al^{3+} compound which has a significantly shorter O1(a2)—O1(b1) edge.

In general, the shared edges expand less than the unshared edges when larger cations are substituted to the M1 site. The ratio between unshared and shared edges e_u/e_s

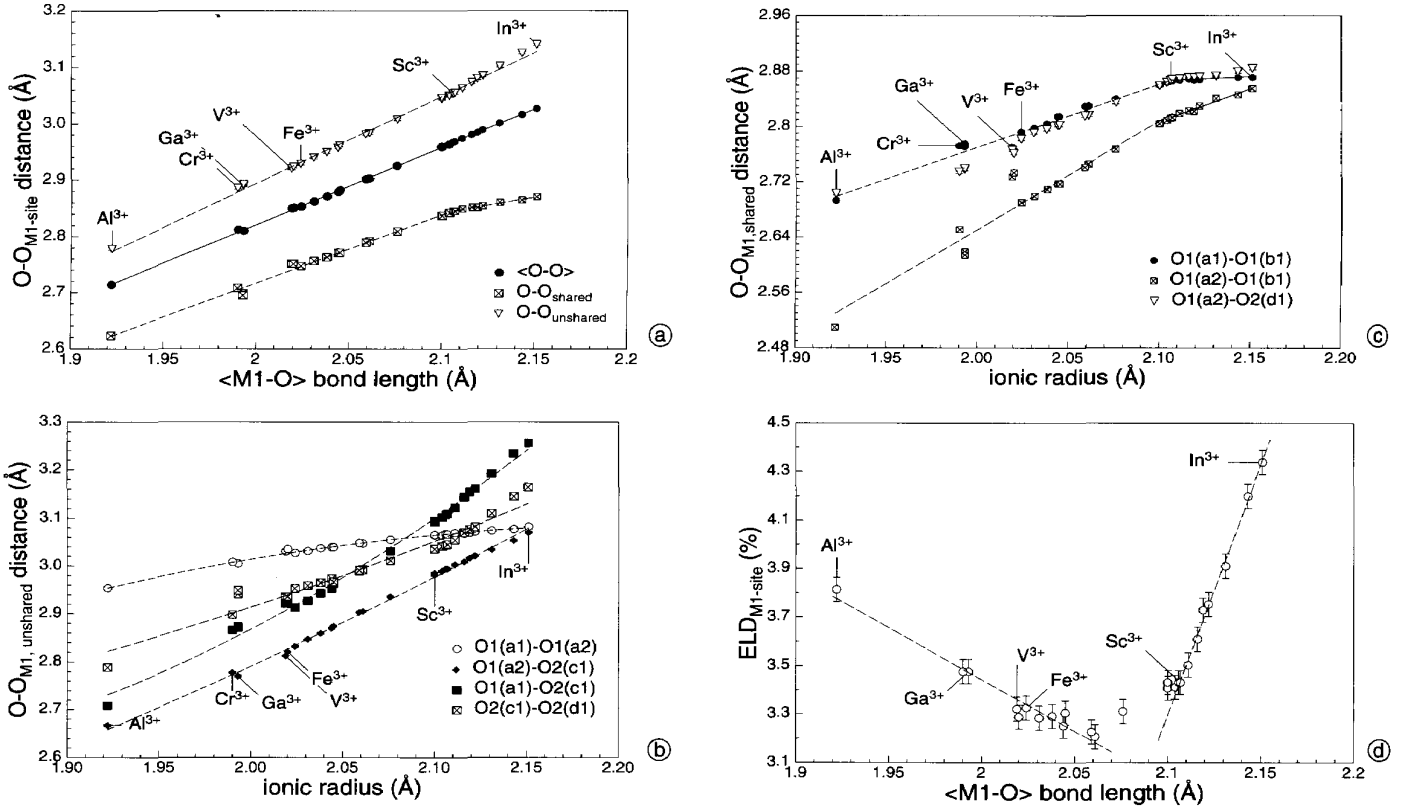

Fig. 5. Oxygen atom interatomic distances (O—O) defining edges of the M1-octahedron for the $LiMe^{3+}Si_2O_6$ series at 295 K. Error bars are smaller than the symbols if not visible; regression lines are fitted to the data as a guide to the eye. (**a**) average values for the M1 O—O distances, (**b**) individual values for the unshared O—O edges, (**c**) individual values for the shared O—O edge (**d**) edge lengths distortion (ELD).